Polymer Chemistry

ROYAL SOCIETY OF CHEMISTRY

PAPER

View Article Online
View Journal | View Issue

Check for updates

Cite this: *Polym. Chem.*, 2021, **12**, 5364

Synthesis and characterization of amide-bridged colorless polyimide films with low CTE and high optical performance for flexible OLED displays†

Zhenghui Yang,[a,b] Haiquan Guo, *[a] Chuanqing Kang [a,b] and Lianxun Gao[a]

Received 7th June 2021,
Accepted 26th August 2021

DOI: 10.1039/d1py00762a

rsc.li/polymers

Three novel dianhydride monomers involving amide groups were synthesized and further polymerized with various diamines to afford a series of colorless polyimides (cPI). The resultant cPI films present outstanding optical performance, exceedingly good dimensional stability at high temperature, great film ductility and solution-processability. In particular, chemically imidized AMDA/TFDB has an ultra-low coefficient of thermal expansion value of 5.2 ppm K^{-A}, a relatively high T_g value of 333 °C and large elongation at break of 29%, resulting from its rigid-rod backbone and the formation of hydrogen bonding (–C═O···NH–) between adjacent molecular chains. Concurrently, it exhibits a high optical transmittance of 87% at a wavelength of 550 nm, a small haze value of 0.71 and low yellow index of 4.29 by reason that the incorporation of bulky trifluoromethyl and cyclohexyl preclude the formation of a charge transfer complex effectively. The high overall performance of the amide-containing cPI films suggests its potential application in the field of flexible OLED displays.

Published on 26 August 2021. Downloaded on 2/20/2026 2:46:30 PM.

1. Introduction

Over the past few decades, thin, flexible organic light-emitting diode (FOLED) displays with high brightness, a wide viewing angle, and a fast response time have become popular for the replacement of glass-based components (*e.g.*, cover window, touch sensor panel or substrate) with transparent polymer materials to keep the entire devices flexible, foldable and even stretchable.[1–3] At present, commercially available transparent polymer films include polyethylene terephthalate,[4,5] polyethylene naphthalate,[6,7] polycarbonate,[8,9] colorless polyimide (cPI)[10–13] and so forth. Among them, cPI is reckoned to be the most promising transparent polymer film for flexible organic light-emitting diode devices because of its excellent heat resistance.[14] However, there are so far no reliable cPIs that also provide high optical transparency ($T_{550\ nm}$ > 87%), ultralow coefficient of thermal expansion (CTE < 10 ppm K^{-1}) and high glass transition temperature (T_g > 300 °C). Generally, the formation of an intra- or intermolecular charge transfer complex (CTC) between electron-accepting dianhydride and electron-donating diamine can result in a deep coloration of polyimide films, that is, the films exhibit poor transparency in the visible light region.[15] To overcome the drawback of deep coloration, bulky substituent groups with high electronegativity (*e.g.*, trifluoromethyl group, sulphone group and so on)[16–18] or aliphatic units (*e.g.*, cyclohexyl group)[19–23] can be introduced into the polyimide molecular chains to decrease and even eliminate the CTC effect. Nevertheless, the incorporation of bulky trifluoromethyl group (–CF_3) can increase the free volume of polyimide and disrupt the coplanarity and linearity of molecular chains so that the CTE was markedly increased resulting in the warpage, cracking, delamination, and other failures in flexible organic light-emitting diode displays.[12,17] When an aliphatic moiety is involved with dianhydride, the poly(amic acid)s (PAAs) suffer from low inherent viscosity and low molecular weight due to the decreased reactivity of dianhydride, which tends to attenuate the comprehensive performance of as-synthesized polyimides.[24] Besides, the incorporation of aliphatic diamine is likely to trigger salt formation at the initial stage of PAAs for which the polymerization reaction is retarded and even terminated.[25,26] In addition to optical transparency, an ultralow CTE is desirable to achieve quite small dimensional changes along the direction (*X*–*Y*) parallel to films at elevated temperature. Some approaches have been reported to decrease the CTE values of polyimide films based on the introduction of linear rigid-rod structure or/and the formation of hydrogen bonds between molecular chains, *etc.*[27–31] However, the optical

[a]*State Key Laboratory of Polymer Physics and Chemistry, Changchun Institute of Applied Chemistry, Chinese Academy of Sciences, Changchun 130022, China. E-mail: hqguo@ciac.ac.cn*
[b]*University of Science and Technology of China, Hefei 230026, China*

† Electronic supplementary information (ESI) available: ^{1}H NMR, ^{13}C NMR, mass spectra of dianhydride monomers; FTIR, TMA, XRD, DMA, GPC, UV-visible spectra and stress–strain curves of several cPI films. See DOI: 10.1039/d1py00762a

This journal is © The Royal Society of Chemistry 2021

Published on 26 August 2021. Downloaded on 2/20/2026 2:46:30 PM.

transparency is sacrificed more often than not when accompanied by reduced CTE values, such as PMDA/TFMB (−4.7 ppm K^{-1}, $T_{400\ nm}$ = 0%, highly colored film)[32] and s-BPDA/TFMB (34 ppm K^{-1}, $T_{400\ nm}$ = 42%, slightly colored film).[33] Also, it is very hard to realize the expected CTE values (<10 ppm K^{-1}). Overall, a reasonable trade-off between optical transparency and CTE should be taken into account for the structure design of cPIs. And some totally rigid molecular chains lead to inferior flexibility (that is, low elongation at break ε_b) of the cPI films with a decreased CTE (*i.e.*, CBDA/DABA: CTE = 9.3 ppm K^{-1}, ε_b = 3%; CBDA/TFMB: CTE = 20.7 ppm K^{-1}, ε_b = 5%).[34] In fact, the excellent ductility of cPI films has become indispensable to flexible OLED displays that need to work under bending, folding and even stretching conditions. Hence, the research for cPI films endowed simultaneously with high optical transparency, low CTE value and superior flexibility is a burning issue in the field of flexible OLED displays.

In this work, three kinds of novel anhydride monomers involving amide groups were synthesized (Scheme 1) and denoted as AMDA, IAMDA, and *p*-DAMDA, respectively. To remove deep coloration and decrease the CTE value, the two diamine monomers TFMB and *t*-CHDA were chosen to polymerize with each of the as-synthesized dianhydrides, and the structure–property relationship of the resulting cPI films was investigated. On the basis of the formation of hydrogen bonds derived from amide groups, the CTE values could be reduced effectively and the presence of trifluoromethyl or cyclohexyl group ensured sufficient optical transparency. Besides this, the heat resistance and mechanical performance of the as-synthesized cPI films were evaluated.

2. Experimental

2.1 Materials

Trimellitic anhydride chloride (TMAC), acetic anhydride and 4-nitrophthalic acid were purchased from SaEn Chemical Technology Co. Ltd. Pyridine and *p*-phthaloyl dichloride were supplied by Shanghai Aladdin Biochemical Technology Co. Ltd. The solvents including toluene, dichloromethane (CH_2Cl_2), ethanol, acetonitrile (CH_3CN), tetrahydrofuran (THF) and *N*,*N*-dimethylacetamide (DMAc) were obtained from Tianjin Fuyu Fine Chemical Co. Ltd. Acetic anhydride was procured from Sinopharm Chemical Reagent Co. Ltd. *trans*-1,4-Diaminocyclohexane (*t*-CHDA) was bought from Regent Science Industry Co. Ltd and purified by sublimation before use. The catalyst Pd/C (10%) was purchased from Shanxi Kaida Chemical Co. Ltd. 2,2′-Bis(trifluoromethyl)benzidine (TFDB) was provided by Changzhou Sunlight Pharmaceutical Co. Ltd and was further sublimated for purification.

2.2 Measurements

Fourier-transform infrared (FTIR) spectra were recorded on a Bruker Vertex 70 FTIR spectrometer. A Rigaku wide-angle X-ray diffractometer (D/max 2500 PC) with Cu Kα radiation (λ = 1.5418 Å) was utilized to obtain wide-angle X-ray diffraction (WAXD) patterns. The parameter 2θ was measured in the range of 5–50°. Dynamic mechanical analysis (DMA) was performed using a TA Instruments DMA Q800 with a heating rate of 10 °C min^{-1}. Thermomechanical analysis (TMA) was conducted on a TMA Q400 instrument with a heating rate of 5 °C min^{-1} in a nitrogen flow to examine the CTE in the range from 50 to 250 °C. Prior to starting the measurement, the samples were firstly heated to 250 °C to eliminate the residual stress. Mechanical properties were evaluated at room temperature using an Instron 1121 universal testing apparatus with a crosshead speed of 5 mm min^{-1}. In this case, the Young's modulus (E_t), maximum tensile strength (σ_m) and elongation at break (ε_b) were calculated as the average over five strips for each group of samples. The thermal properties were determined by thermogravimetric analysis (TGA, PerkinElmer) with a heating rate of 10 °C min^{-1} under N_2 in the temperature range from 50 to 800 °C. The in-plane (n_{TE}, transverse electric mode) and out-of-plane (n_{TM}, transverse magnetic mode) refractive indices were measured at a wavelength of 632.8 nm by a prism coupler (Metricon 2010). Color intensity and optical transmittance were evaluated with a CM-3600A spectrophotometer (Konica

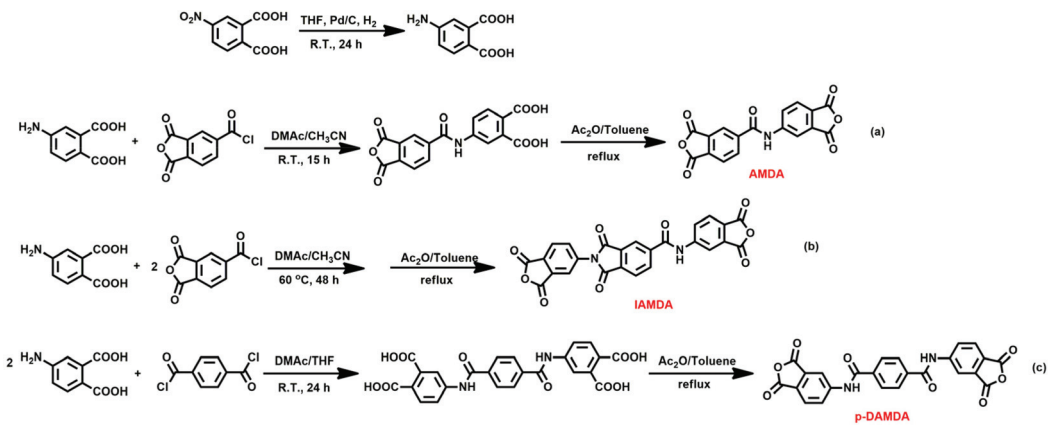

Scheme 1 Synthetic routes to three dianhydride monomers: (a) AMDA; (b) IAMDA; (c) *p*-DAMDA.

Published on 26 August 2021. Downloaded on 2/20/2026 2:46:30 PM.

Minolta) and a UV-2550 spectrophotometer (Shimadzu), respectively. The inherent viscosity of PAAs was measured at a concentration of 0.5 g dL^{-1} in DMAc at 30 °C. The molecular weight of cPI films was measured by gel permeation chromatography (GPC) in DMF.

2.3 Synthesis of dianhydride monomers

The amide-containing dianhydride monomers were synthesized on the basis of the reactions displayed in Scheme 1.

4-Aminophthalic acid. Under hydrogen atmosphere, 4-nitrophthalic acid (100 g, 0.4736 mol) was dissolved in THF (2.5 L) and the mixture was stirred vigorously in the presence of Pd/C (10 g) for 24 h at room temperature. Afterwards, the catalyst Pd/C was removed by filtration and the solution was concentrated under reduced pressure to afford off-white solid (98 g, 98%) that was vacuum-dried at 50 °C for 24 h. ^{1}H NMR (300 MHz, DMSO): δ = 12.44 (s, 2H), 7.53 (d, J = 8.5, 1H), 6.61–6.48 (m, 2H), 6.01 (s, 2H).

AMDA. To a solution of TMAC (10.5285 g, 0.05 mol) dissolved in DMAc/CH_3CN (30 g/10 g) was added 4-aminophthalic acid (9.0575 g, 0.05 mol) at room temperature. After stirring for 15 h, the solution was filtered to obtain a white solid (13.35 g, yield: 75%) washed by CH_2Cl_2. The obtained white product was added to a mixture of Ac_2O (38.36 g, 0.3758 mol) and toluene (100 g) that was refluxed at 120 °C for 5 h. After cooling to room temperature, the solution was filtered to obtain the target product AMDA (8.8 g, yield: 70%, m.p. = 220 °C) that was dried under vacuum at 160 °C for 10 h. ^{1}H NMR (400 MHz, DMSO): δ 11.31 (s, 1H), 8.64 (s, 1H), 8.54–8.49 (m, 2H), 8.27 (d, J = 8.0, 2H), 8.12 (d, J = 8.3, 1H). ^{13}C NMR (101 MHz, DMSO): δ 164.2, 163.2, 162.7, 162.6, 162.5, 145.6, 140.5, 135.8, 134.1, 132.8, 131.7, 126.7, 126.6, 125.6, 125.5, 124.3, 115.3. FTIR (KBr, cm^{-1}): 3363 (–NH– stretching), 1849 (*asym* C═O stretching from the moiety –CO–O–CO–), 1774 (*sym* C═O stretching from the moiety –CO–O–CO–), 1688 (C═O stretching from the moiety –CONH–), 1534 (–NH– bending vibration).

IAMDA. To a solution of TMAC (2.1057 g, 0.01 mol) in a mixed solvent of DMAc/CH_3CN (5 g/50 g) was added 4-aminophthalic acid (3.623 g, 0.02 mol). The reaction mixture was stirred for 48 h at 60 °C and then a white solid product (3.79 g, yield: 71%) was obtained by filtration. Afterwards, the obtained white powder was blended with Ac_2O (7.21 g, 0.07 mol) and toluene (50 g) thoroughly. After stirring for 5 h at 120 °C, the solution was cooled down to room temperature and then was filtered to obtain white product (2.76 g, yield: 82%, m.p. = 298 °C) that was vacuum-dried at 160 °C for 10 h. ^{1}H NMR (300 MHz, DMSO): δ 11.31 (s, 1H), 8.64 (s, 1H), 8.56–8.49 (m, 2H), 8.33–8.26 (m, 2H), 8.21 (dd, J = 12.8, 4.5, 2H), 8.12 (dd, J = 8.2, 1.7, 2H). ^{13}C NMR (101 MHz, DMSO): δ 165.7, 165.6, 164.4, 163.2, 162.6, 145.7, 139.5, 138.3, 135.0, 134.2, 133.9, 132.7, 132.3, 131.7, 130.1, 126.7, 126.5, 126.1, 125.4, 124.1, 123.0, 122.8, 115.3. FTIR (KBr, cm^{-1}): 3370 (–NH– stretching), 1855 (*asym* C═O stretching from the moiety –CO–O–CO–), 1781 (*sym* C═O stretching from the moiety –CO–O–CO–), 1729 (C═O stretching from the moiety –CO–N–CO–), 1680 (C═O stretching from the moiety –CONH–), 1545 (–NH– bending vibration), 1354 (–C–N–C– stretching of imide ring).

***p*-DAMDA.** To a solution of *p*-phthaloyl dichloride (4.0604 g, 0.02 mol) dissolved in DMAc/THF (30 g/30 g) was added 4-aminophthalic acid (7.246 g, 0.04 mol) and the mixture was stirred vigorously for 24 h at room temperature before the white solid product (8.4 g, yield: 85%) was separated from the solvent by filtration and evaporation under reduced pressure. The collected white product was refluxed with Ac_2O (8.7 g, 0.085 mol) and toluene (60 g) at 120 °C for 5 h, after which the white product (6.1 g, yield: 78%, m.p. = 393 °C) was obtained by filtering and was dried under vacuum at 160 °C for 10 h. ^{1}H NMR (400 MHz, DMSO): δ 11.31 (s, 1H), 8.64 (s, 1H), 8.54–8.49 (m, 2H), 8.27 (d, J = 8.0, 2H), 8.12 (d, J = 8.3, 1H). ^{13}C NMR (101 MHz, DMSO): δ 165.6, 163.3, 162.7, 146.2, 136.7, 132.6, 128.3, 126.7, 126.4, 125.0, 115.3. FTIR (KBr, cm^{-1}): 3374 (–NH– stretching), 1841 (*asym* C═O stretching from the moiety –CO–O–CO–), 1774 (*sym* C═O stretching from the moiety –CO–O–CO–), 1664 (C═O stretching from the moiety –CONH–), 1544 (–NH– bending vibration).

2.4 Synthesis of cPI films

A series of transparent PAAs were fabricated from the reaction of dianhydrides and diamines as shown in Scheme 2. The cPI films were successfully afforded *via* chemical or thermal imidization of PAA films. Concerning the TFDB-based cPI films, taking AMDA/TFDB as an example, AMDA (2.3607 g, 0.007 mol) was added to a solution of TFDB (2.2416, 0.007 mol) dissolved in DMAc (18.40 g) and the mixture was continuously stirred for 24 h under nitrogen atmosphere at room temperature. Subsequently, acetic anhydride (7.1463 g, 0.07 mol) and pyridine (5.537 g, 0.07 mol) were slowly added into the PAA. After stirring adequately for 24 h, the reactive mixture was diluted with DMAc (30 g) and then slowly poured into a great quantity of anhydrous ethanol to produce a fibrous white resin that was dried in vacuum for 10 h at 100 °C. The transparent and clear solution was prepared by redissolving the dried cPI resin into the solvent DMAc (solid content: 10%) and was cast onto a clean glass substrate by an automatic film applicator, followed by being dried at 70 °C for 3 h in an air-convection oven and 150 °C for 2 h in a vacuum oven. With regard to the *t*-CHDA-based cPI films, taking AMDA/*t*-CHDA as an example, acetic acid (1.4412 g, 0.024 mol) was added dropwise to a solution of *t*-CHDA (1.3703 g, 0.012 mol) dissolved in DMAc (22 g) and the mixture was stirred for 10 min at room temperature. Then, AMDA (4.0042 g, 0.012 mol) was put into the reaction system in order to polymerize with *t*-CHDA. After stirring for 24 h at room temperature, the afforded colorless PAA was cast onto a clean glass substrate by an automatic film applicator and dried at 70 °C for 3 h in an air-convection oven before the precursor films underwent thermal imidization in vacuum with a programmed temperature procedure of 100 °C (0.5 h)/150 °C (0.5 h)/200 °C (0.5 h)/250 °C (1 h).

 This journal is © The Royal Society of Chemistry 2021

Published on 26 August 2021. Downloaded on 2/20/2026 2:46:30 PM.

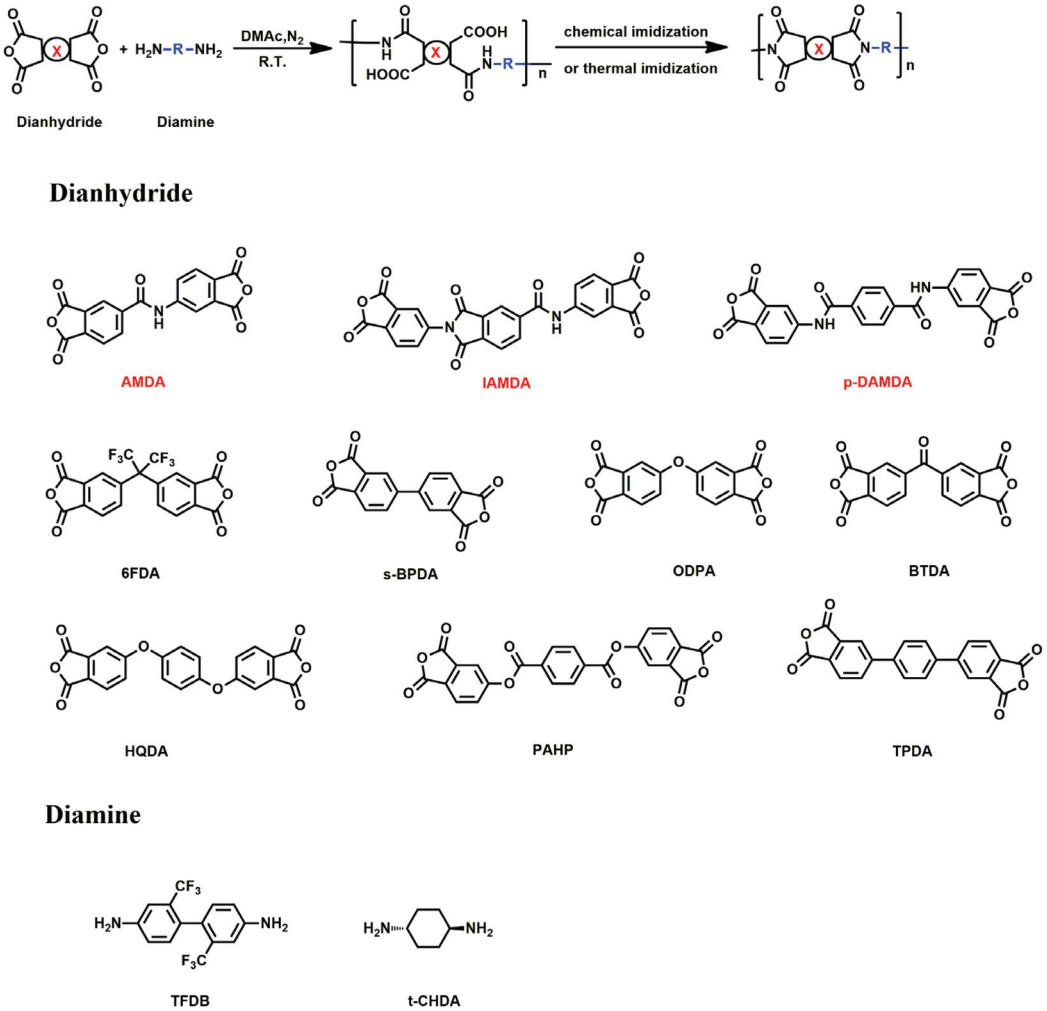

Scheme 2 Synthesis of poly(amic acid)s (PAAs) and polyimides.

3. Results and discussion

3.1 Structural characteristics of dianhydride monomers

As shown in Scheme 1, three novel dianhydride monomers were synthesized through a three-step procedure involving hydrogenation under high pressure, amidation reaction, and dehydration with acetic anhydride. The structural characterization of the dianhydride monomers was realized from mass spectra, ^{1}H NMR spectra, ^{13}C NMR spectra (Fig. S1–S9) and FTIR spectra. The signal of proton derived from amide group (δ = 11.31 ppm) was observed in the ^{1}H NMR spectra for AMDA, IAMDA and *p*-DAMDA, while the signal of carboxylic acid protons was absent from ^{1}H NMR spectra, implying the completion of both amidation and dehydration. From the FTIR spectra of the dianhydride monomers (Fig. S16†), the –NH– stretching of amide group was located at 3363 cm^{-1} for AMDA, 3370 cm^{-1} for IAMDA and 3374 cm^{-1} for *p*-DAMDA. Furthermore, the C=O stretching and –NH– bending vibrations in amide group were observed in the range of 1688–1664 cm^{-1} and 1534–1545 cm^{-1}, respectively. The results indicated the amide group was successfully incorporated within the dianhydride monomers. Unlike the other two dianhydrides, IAMDA has an imide ring so that the characteristic peaks of C–N–C stretching and C=O stretching could be observed at 1354 cm^{-1} and 1729 cm^{-1}, respectively. Additionally, for the three dianhydride monomers, the asymmetrical and symmetrical stretching of carbonyl group from the –CO–O–CO– moiety were located in the range of 1841–1855 cm^{-1} and 1774–1781 cm^{-1}, respectively.

3.2 Synthesis and structural characteristics of the cPI films

A series of amide-bridged cPI films were synthesized *via* a traditional two-step method. It was noteworthy that gelation occurred at the PAA stage when *p*-DAMDA was added to a solution of *t*-CHDA dissolved in DMAc, even in the presence of acetic acid, benzoic acid or bromoacetic acid. The number-average molecular weight (M_n) and weight-average molecular weight (M_w) of AMDA/TFDB were 25.5 × 10^4 g mol^{-1} and 36.0 × 10^4 g mol^{-1}, respectively (Table S1†). Analogously, M_n and M_w of IAMDA/TFDB were 22.1 × 10^4 g mol^{-1} and 32.9 × 10^4 g

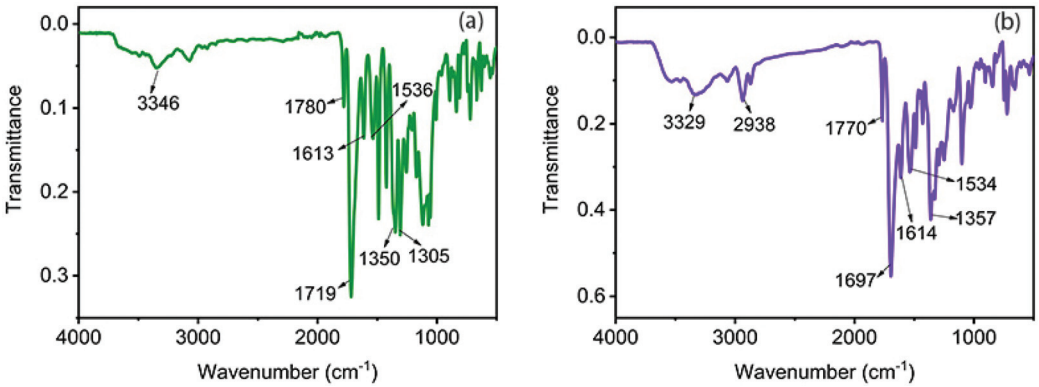

Fig. 1 FTIR spectra of the cPI films: (a) AMDA/TFDB; (b) AMDA/*t*-CHDA.

Published on 26 August 2021. Downloaded on 2/20/2026 2:46:30 PM.

mol^{-1}, respectively. Moreover, AMDA/TFDB and IAMDA/TFDB had low polymer dispersity index (PDI) of 1.40 and 1.48, respectively. The results elucidated that both AMDA/TFDB and IAMDA/TFDB presented with high molecular weight and narrow molecular weight distribution. Along with this, the inherent viscosity (η_{inh}) of AMDA/TFDB and IAMDA/TFDB was 1.93 dL g^{-1} and 1.80 dL g^{-1}, respectively. The other cPI films, including *p*-DAMDA/TFDB, AMDA/*t*-CHDA and IAMDA/*t*-CHDA, showed poor solubility in DMF. Therefore, the inherent viscosity of PAAs was measured to evaluate the molecular weight. Three kinds of PAAs had relatively high molecular weight with inherent viscosity in the range of 0.56–1.20 dL g^{-1} (Table S2†).

The structure of colorless polyimides was determined from their FTIR spectra. With respect to AMDA/TFDB (Fig. 1a), the formation of imide ring was supported by the presence of the characteristic peak at 1350 cm^{-1} that was attributed to C–N–C stretching. Besides, the typical absorption peaks at 1780 cm^{-1} and 1719 cm^{-1} were assigned to the asymmetrical and symmetrical stretching vibration of carbonyl group (C═O) from the imide ring, respectively. Meanwhile, the broad absorption band at 3346 cm^{-1} corresponded to the –NH– stretching of amide group for which the C═O stretching band was located at 1613 cm^{-1} and 1536 cm^{-1}.[34] Moreover, the strong absorption peak at 1305 cm^{-1} was assigned to C–F stretching.[35] For AMDA/*t*-CHDA (Fig. 1b), the typical absorption peaks of phthalimide moiety were located at 1770 cm^{-1} (ν_{asym} C═O), 1697 cm^{-1} (ν_{sym} C═O) and 1357 cm^{-1} (imide, C–N–C) while the presence of amide group was confirmed by the characteristic peaks at 3329 cm^{-1} (–NH– stretching) and 1614 cm^{-1}/1534 cm^{-1} (C═O stretching). Additionally, the absorption peak at 2938 cm^{-1} corresponded to methylene ($-CH_2-$) stretching of cyclohexyl unit. The spectra of the other cPI films had analogous characteristic peaks to those of AMDA/TFDB and AMDA/*t*-CHDA. The FTIR results were as follows.

IAMDA/TFDB. 3338 cm^{-1} (–NH– stretching of amide group), 1782 cm^{-1} (*asym* C═O stretching of imide ring), 1720 cm^{-1} (*sym* C═O stretching of imide ring), 1615/1545 cm^{-1} (C═O stretching of amide group), 1350 cm^{-1} (C–N–C stretching of imide ring), 1305 cm^{-1} (C–F stretching).

IAMDA/*t*-CHDA. 3346 cm^{-1} (–NH– stretching of amide group), 2938 cm^{-1} ($-CH_2-$ stretching), 1770 cm^{-1} (*asym* C═O stretching of imide ring), 1697 cm^{-1} (*sym* C═O stretching of imide ring), 1615/1537 cm^{-1} (C═O stretching of amide group), 1354 cm^{-1} (C–N–C stretching of imide ring).

***p*-DAMDA/TFDB.** 3334 cm^{-1} (–NH– stretching of amide group), 1778 cm^{-1} (*asym* C═O stretching of imide ring), 1713 cm^{-1} (*sym* C═O stretching of imide ring), 1611/1534 cm^{-1} (C═O stretching of amide group), 1346 cm^{-1} (C–N–C stretching of imide ring), 1305 cm^{-1} (C–F stretching).

3.3 Optical properties of the cPI films

Optical performances are well known to be of vital importance for cPI films as cover windows, touch sensor panels or substrates of OLED displays, and were herein characterized by optical transmittance at a wavelength of 550 nm ($T_{550\ nm}$), cut-off wavelength ($\lambda_{cut\text{-}off}$), turbidity (haze) and yellowness index (YI). As shown in Fig. 2, the cPI films exhibited high optical transmittance ($T_{550\ nm}$ > 85%), especially AMDA/TFDB and AMDA/*t*-CHDA that had $T_{550\ nm}$ value of 87%. The cut-off wavelength of the cPI films was located in the range of 380–391 nm. For the same polymer backbone, the cPI film prepared by means of chemical imidization presented a smaller $\lambda_{cut\text{-}off}$ value than that prepared by thermal imidization (Table 1). The color intensity of these cPI films is summarized in Table 1. All of the cPI films showed high L^* value (>94) implying excellent lightness, and had b^* values in the range of 1.84–5.48 indicating light coloration and good transparency.[36] Additionally, these films had small and negative a^* values indicating the presence of a greenish tinge,[37] and showed relatively low haze values in the range of 0.39–1.37. The optical transparency, degree of coloration and turbidity of the cPI films were strongly affected by the chemical structure of polyimide chains wherein the inter- and intramolecular charge transfer interaction could lead to a new absorption band in the visible light region.[38] In consideration of steric hindrance and inductive effects, the incorporation of bulky trifluoromethyl group ($-CF_3$) and cyclohexyl group contributed to perturbing inter- and intramolecular CTC formation and thus

 This journal is © The Royal Society of Chemistry 2021

Published on 26 August 2021. Downloaded on 2/20/2026 2:46:30 PM.

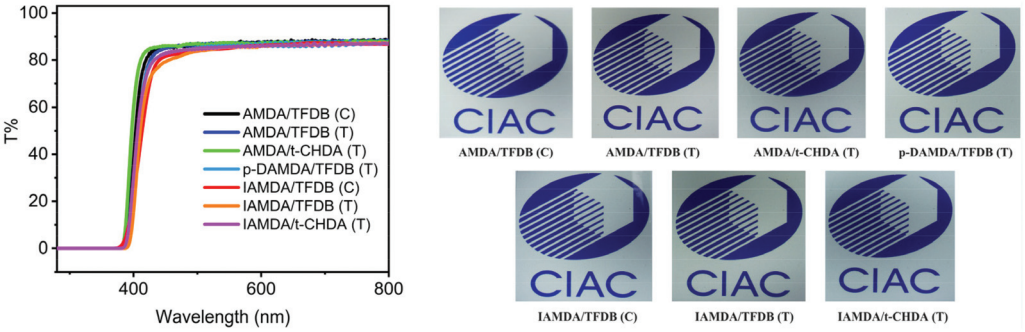

Fig. 2 UV-visible transmission spectra and images of the cPI films.

Table 1 Optical properties of the as-synthesized cPI films

Polymer	Imidization method[a]	Thickness (μm)	$\lambda_{cut\text{-}off}$ (nm)	$T_{550\ nm}$ (%)	Haze	L^{*b}	a^*	b^*	YI
AMDA/TFDB	C	25	386	87	0.71	94.70	−0.66	2.48	4.29
	T	25	391	87	0.39	95.00	−0.62	2.02	3.43
AMDA/*t*-CHDA	T	26	382	87	0.60	94.87	−0.43	1.84	3.24
p-DAMDA/TFDB	T	22	390	86	0.88	94.16	−1.38	4.53	7.65
IAMDA/TFDB	C	28	380	85	1.37	94.65	−0.86	2.61	4.40
	T	28	391	85	0.97	94.44	−1.83	5.48	9.06
IAMDA/*t*-CHDA	T	21	386	86	1.26	94.68	−1.08	2.91	4.80

[a] C: Chemical imidization; T: thermal imidization. [b] Color parameters are calculated based on the CIE LAB equation. L^* represents the lightness where 100 means white and 0 indicates black. Positive a^* and b^* values imply red color and yellow color, respectively, whereas negative a^* and b^* values refer to green color and blue color, respectively. YI indicates the yellowness index.

gave rise to the high optical performance of the as-synthesized cPI films.

3.4 Thermal dimensional stability of the cPI films

The outstanding dimensional stability of cPI films at elevated temperature is absolutely necessary to keep OLED devices functioning well. Herein, the CTE values were measured by TMA and the impact of the amide group on the CTE values of the cPI films was investigated. As shown in Fig. 3, the CTE values of the as-synthesized cPI films are in the range of 5.2–11.9 ppm K^{-1}, suggesting that a relatively high degree of in-plane orientation took place within the films. To evaluate the in-plane orientation of cPI films, the optical birefringence values (Δn) were calculated with the help of in-plane (n_{TE}, transverse electric mode) and out-of-plane (n_{TM}, transverse magnetic mode) refractive indices. As depicted in Table 2, the chemically imidized AMDA/TFDB had the highest birefringence value (Δn = 0.1363) of all the as-synthesized cPI films, which conformed well to the lowest CTE (5.2 ppm K^{-1}). Comparatively, the other cPI films had lower Δn values at around 0.1 that were basically in accord with the relatively high CTE results. As a matter of fact, the in-plane orientation is highly susceptible to structural linearity/stiffness[39–43] and intermolecular force[44,45] (*i.e.*, hydrogen bonds). Therefore, geometry optimization was conducted using Chemdraw 3D under a MM2 force-field module to obtain the steric structure of the as-synthesized dianhydrides.[29] The backbone angles of the dianhydrides were observed to be in the range of 150–170° (Fig. 4) and the structural linearity decreased in the order of AMDA > IAMDA ≈ *p*-DAMDA. That is to say, the AMDA-containing cPI films showed much better structural linearity of molecular chains than the cPI films involving IAMDA or *p*-DAMDA. As a result, the chemically imidized AMDA/TFDB exhibited lower CTE value at 5.2 ppm K^{-1} than that of IAMDA/TFDB (10.2 ppm K^{-1}). Nevertheless, the thermally imidized TFDB-based cPI films showed distinctly decreased CTE values in the order of IAMDA/TFDB > AMDA/TFDB > *p*-DAMDA/TFDB, which did not completely coincide with the structural linearity. To begin

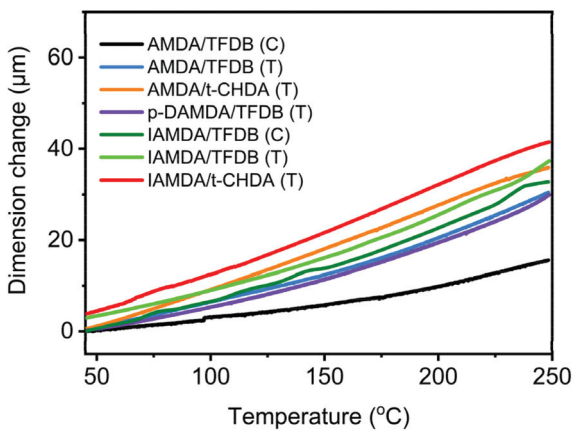

Fig. 3 Dimension changes of the cPI films as a function of temperature.

Published on 26 August 2021. Downloaded on 2/20/2026 2:46:30 PM.

Table 2 Refractive indices and CTE values of homopolymers

Polymer	Imidization method[a]	n_{TE}[b]	n_{TM}	n_{av}	Δn	CTE[c] (ppm K^{-1})
AMDA/TFDB	C	1.6805	1.5442	1.6363	0.1363	5.2
	T	1.6612	1.5571	1.6272	0.1041	9.0
AMDA/*t*-CHDA	T	1.6877	1.5899	1.6557	0.0978	11.3
p-DAMDA/TFDB	T	1.6666	1.5493	1.6284	0.1173	8.7
IAMDA/TFDB	C	1.6823	1.5836	1.6500	0.0987	10.2
	T	1.6808	1.5819	1.6485	0.0989	10.3
IAMDA/*t*-CHDA	T	1.6832	1.5899	1.6526	0.0933	11.9

[a] C: Chemical imidization; T: thermal imidization. [b] n_{TE} and n_{TM} were measured at 632.8 nm; $n_{av} = [(2n_{TE}^2 + n_{TM}^2)/3]^{1/2}$; $\Delta n = n_{TE} - n_{TM}$. [c] CTE values were measured in the temperature range of 50–250 °C.

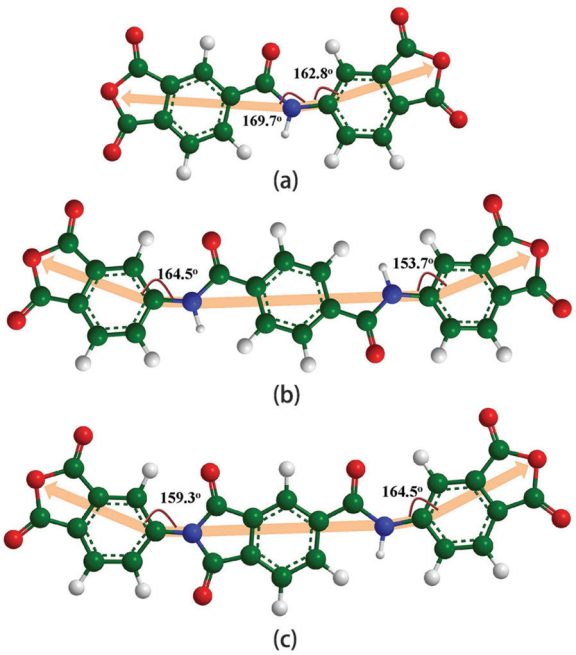

Fig. 4 Optimized structures of (a) AMDA, (b) *p*-DAMDA, and (c) IAMDA.

with, the CTE value of *p*-DAMDA/TFDB at 8.7 ppm K^{-1} was lower than that of the IAMDA/TFDB counterpart (10.3 ppm K^{-1}) although the two dianhydrides in the cPIs presented analogous structural linearity. Next, the AMDA/TFDB film had far greater structural linearity than *p*-DAMDA/TFDB, but it showed a slightly higher CTE value at 9.0 ppm K^{-1} than *p*-DAMDA/TFDB. The results could be explained by the fact that the number of amide groups (–CONH–) within *p*-DAMDA/TFDB was nearly twice more than within IAMDA/TFDB and AMDA/TFDB so that the former had a much greater opportunity to form hydrogen bonds between adjacent molecular chains in comparison with the latter. Moreover, the CTE value of the thermally imidized *t*-CHDA-based cPI films was examined. The CTE values of AMDA/*t*-CHDA and IAMDA/*t*-CHDA were 11.3 ppm K^{-1} and 11.9 ppm K^{-1}, respectively, aligning with the structural linearity order of AMDA/*t*-CHDA > IAMDA/*t*-CHDA.

In addition to structural linearity, the formation of hydrogen bonding between adjacent molecular chains was another crucial factor for suppressing the thermal expansion behavior and reducing CTE value. Herein, a series of cPI films with various connecting groups (C═O, –O–, –COO– and so forth) in the molecular chains were prepared and compared with amide-bridged cPI films to investigate how the amide group affected the dimensional change behavior. Fig. 5a shows the CTE results of TFDB-based cPI films. From the viewpoint of structural characteristics, the s-BPDA/TFDB film with a rigid-rod backbone contained no connecting group and exhibited a relatively low CTE value of 14 ppm K^{-1}, whereas the incorporation of some flexible linkages (*i.e.*, $-C(CF_3)_2-$, C═O, –O–) resulted in a significant increase in the CTE value, such as 56 ppm K^{-1} for 6FDA/TFDB, 49 ppm K^{-1} for BTDA/TFDB, and 66 ppm K^{-1} for ODPA/TFDB. Analogously, it was previously reported[33] that TPDA/TFDB has a CTE value of 37 ppm K^{-1}, lower than those of films involving flexible connecting groups, such as 73 ppm K^{-1} for HQDA/TFDB. In short, incorporating flexible linkages within the totally rigid s-BPDA/TFDB and TPDA/TFDB was generally unfavorable for reduction of CTE value. Nevertheless, in our study, the incorporation of amide group (–CONH–) was found to effectively reduce the CTE to a level below 10 ppm K^{-1} (Fig. 5a). For instance, *p*-DAMDA/TFDB presented a CTE value almost four times lower than that of the TPDA/TFDB counterpart. Meanwhile, the CTE values of amide-bridged cPI films were much less than those of the other cPI films involving flexible connecting groups, suggesting both the great linearity of molecular backbone and formation of hydrogen bonds had a positive effect on the chain alignment. In particular, it was observed that PAHP/TFDB and *p*-DAMDA/TFDB had almost the same linearity of molecular chains but exhibited remarkably different dimension changes. PAHP/TFDB had a much higher CTE value of 29.3 ppm K^{-1} than that of *p*-DAMDA/TFDB (8.7 ppm K^{-1}), which confirmed the validity of hydrogen bonding; that is, the replacement of an ester linkage with an amide group was of great benefit to the CTE reduction of cPI films. Moreover, PAHP/TFDB exhibited a turbid appearance and poor mechanical performance since a high level of crystallization occurred during the process of thermal imidization (Fig. S10†). Research on the comparison of *t*-CHDA-based cPI films showed similar results as depicted in Fig. 5b. The introduction of flexible connecting groups ($-C(CF_3)_2-$, C═O, –O–) led to a significant increase of CTE value exceeding 40 ppm K^{-1} and thus caused serious deterio-

 This journal is © The Royal Society of Chemistry 2021

Published on 26 August 2021. Downloaded on 2/20/2026 2:46:30 PM.

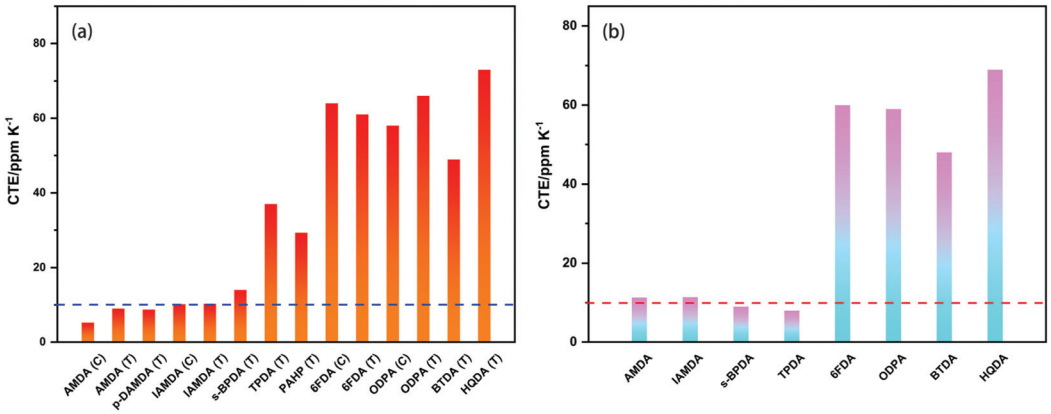

Fig. 5 Comparison of CTE values for (a) TFDB-based cPI films and (b) *t*-CHDA-based cPI films.

ration of thermal dimensional stability, whereas the amide-bridged cPI films had low CTE values rivalling those of s-BPDA/*t*-CHDA and TPDA/*t*-CHDA.

To reveal the formation of hydrogen bonding, a series of copolyimide films (Co-PIs) were synthesized from the reaction of diamine (TFDB) and two dianhydrides (6FDA and AMDA) *via* the chemical imidization. Fig. 6 shows the FTIR spectra of the Co-PIs. With an increase in the AMDA content, the band positions of the asymmetrical and symmetrical carbonyl (C═O) stretching in the imide ring shifted from 1787.2 cm^{-1} and 1726.4 cm^{-1} to 1779.9 cm^{-1} and 1719.7 cm^{-1}, respectively. The results suggested a red shift of the C═O band occurred with the incorporation of amide groups, which has been previously reported[29] to take place upon the formation of hydrogen bonds. This confirmed the presence of hydrogen bonding (–C═O···NH–) between the C═O groups of the imide rings and N–H units of the amide group (Scheme 3a). Concurrently, the characteristic peak of C═O stretching of the amide group was shifted from 1616.7 cm^{-1} to 1613.3 cm^{-1}, indicating another hydrogen-bonding formation (Scheme 3b) caused by the interaction between two amide groups. Besides this, the dimensional change behavior of Co-PIs was further examined and the results are displayed in Fig. 7. As the AMDA content was increased, the CTE value obviously reduced from 56 ppm K^{-1} to 15 ppm K^{-1} while very good optical transmittance (>87%) and high T_g value (>340 °C) were well preserved (Table S3, Fig. S11–S13†). It turned out that two kinds of hydrogen bonds were indeed present between adjacent molecular chains due to the incorporation of amide groups and further performed a critical role in the reduction of the CTE values.

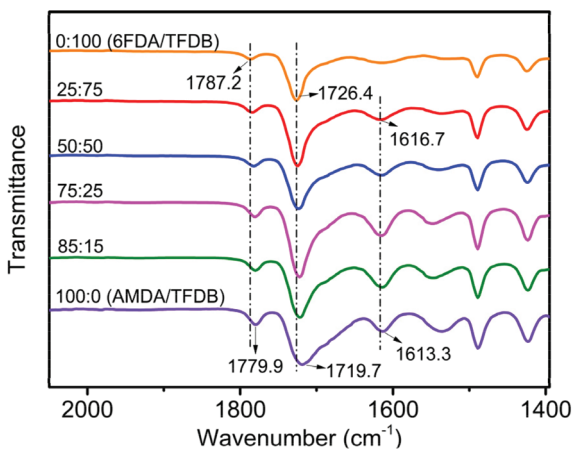

Fig. 6 FTIR spectra of copolyimide films based on dianhydride (AMDA and 6FDA) and diamine TFDB. (The molar ratio of AMDA/6FDA = 0/100; 25/75; 50/50; 75/25; 85/15; 100/0.)

3.5 Thermal properties of the cPI films

As shown in Fig. 8a, the cPI films exhibited a drastic reduction in the storage modulus (E') around 300 °C, indicating the appearance of obvious glass transition behavior. Correspondingly, the T_g values of cPI films were observed in the range of 333–356 °C (Fig. 8b). In general, the glass transition behavior of polyimide films depends on the rigidity and linearity of main chains coupled with intermolecular force. The incorporation of bulky –CF_3– and nonplanar cyclohexyl groups could cause a significant increase in the distance between the adjacent molecular chains and largely weaken the intermolecular force, which was supported by the broad diffraction peak obtained from WAXD patterns (Fig. S14†). In spite of this, the as-synthesized cPIs were equipped with highly rigid and linear molecular chains, which was of benefit to strengthening the intermolecular force and resulting in a decrease in the T_g value. Additionally, the presence of hydrogen bonds between adjacent molecular chains exerted a positive effect on the enhancement of the T_g value.

The thermal decomposition behavior of the cPI films was examined using TGA in the temperature range of 50–800 °C and was characterized by the 5% weight loss temperature ($T_{d5\%}$) and the residual weight percentage at 800 °C (R_w). From the TGA curves (Fig. 9), the $T_{d5\%}$ value of the cPI films was observed in the range of 456–502 °C and the major thermal decomposition occurred in the temperature region of 450–650 °C, suggesting great thermal stability. Additionally,

Published on 26 August 2021. Downloaded on 2/20/2026 2:46:30 PM.

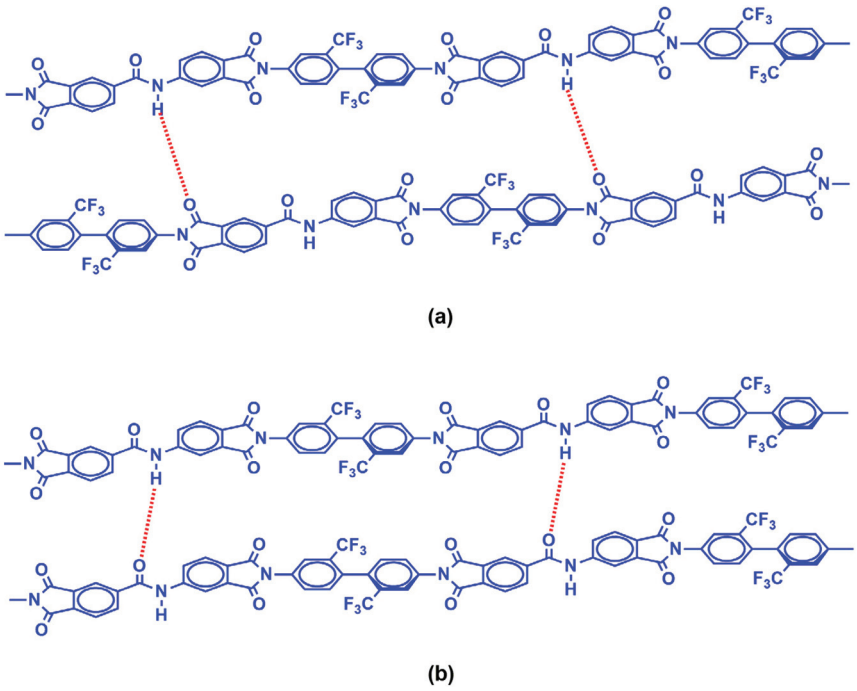

Scheme 3 Hydrogen-bonding formation: (a) between the C═O moiety of the imide ring and the N–H unit of the amide group; (b) between two amide groups.

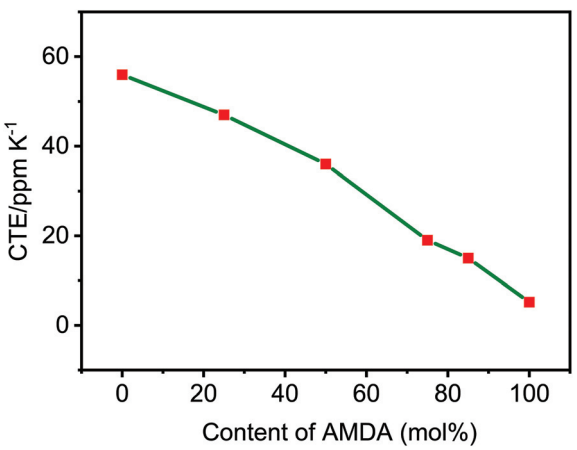

Fig. 7 CTE value of the copolyimide films (6FDA/AMDA/TFDB) as a function of AMDA content.

the TFDB-based cPI films (AMDA/TFDB, *p*-DAMDA/TFDB, IAMDA/TFDB) had a relatively high char yield (R_w > 49%), whereas the *t*-CHDA-based cPI films, including AMDA/*t*-CHDA and IAMDA/*t*-CHDA, exhibited R_w values lower than 26%, which was mainly attributed to the inferior thermal stability of the alicyclic units.[46,47]

3.6 Mechanical properties of the cPI films

The mechanical properties of cPI films are summarized in Table 3. The tensile strength, tensile modulus and elongation at break of cPI films were in the ranges of 144–193 MPa, 1.8–3.9 GPa, and 9.0%–46%, respectively. Particularly, the chemically imidized cPI films exhibited tensile strength and flexibility much higher than that of thermally imidized cPI films. Taking AMDA/TFDB as an example, the AMDA/TFDB(T) film had less ductility (ε_b = 10%) and lower tensile strength (σ_m = 164 MPa) than the AMDA/TFDB(C) counterpart, the elongation at break and tensile strength of which were 29% and 193 MPa, respectively (Fig. S15†). Generally, the mechanical performance of the cPI films correlated with an aggregated structure.[29] The chemically imidized cPI films displayed a much higher degree of imidization than the thermally imidized cPI films resulting in dense stacking and greater chain entanglement, which was beneficial to improving the mechanical performance. To sum up, the cPI films, especially the two AMDA/TFDB(C) and IAMDA/TFDB(C) films, had superior tensile strength and sufficient flexibility for application as cover windows, touch sensor panels or substrates in the field of OLED displays.

To evaluate the overall performance of the as-synthesized cPI films, comparisons were made of optical transmittance, T_g and CTE value between the amide-bridged cPI films in our work and other conventional TFDB- or *t*-CHDA-based cPI films and the results are plotted in Fig. 10. As we can see, the optical transmittance and T_g value of most conventional TFDB- or *t*-CHDA-based cPI films range from 83% and 245 °C to 90% and 344 °C, respectively, indicating good optical performance and great heat resistance. Despite this, those films still had high CTE values reflecting the poor thermal dimensional stability. In contrast, amide-bridged cPI films embodied the features of high optical transmittance, great heat resistance and

 This journal is © The Royal Society of Chemistry 2021

Published on 26 August 2021. Downloaded on 2/20/2026 2:46:30 PM.

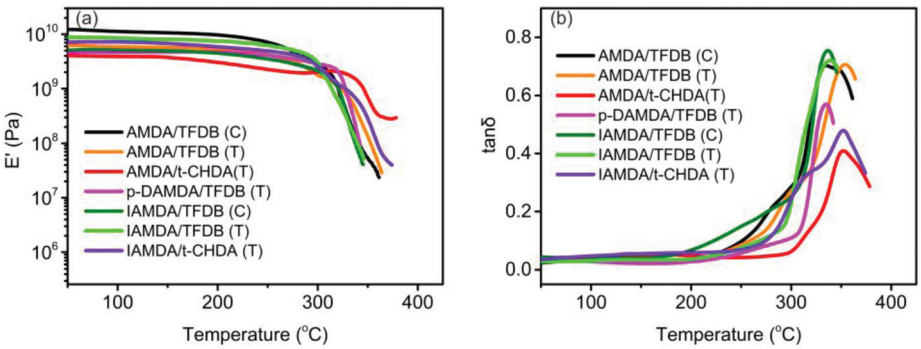

Fig. 8 (a) Storage moduli and (b) tan δ values of the cPI films as a function of temperature.

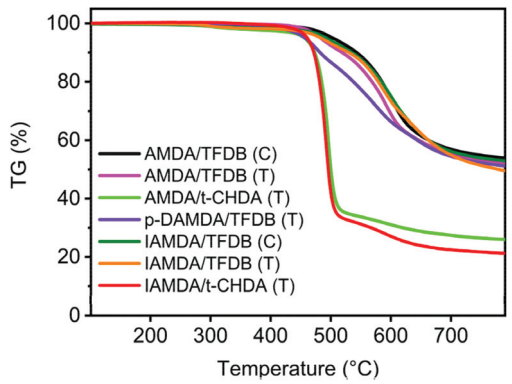

Fig. 9 Weight loss of the cPI films as a function of temperature.

superior dimensional stability at elevated temperature, especially 5.2 ppm K^{-1} for AMDA/TFDB(C), which exceeded that of conventional TFDB-based cPI films. It is concluded that the overall performance of the amide-bridged films was much better than that of the conventional TFDB- or *t*-CHDA-based cPI film counterparts due to the introduction of amide linkages.

4. Conclusion

Three novel dianhydride monomers involving amide groups were synthesized and further reacted with various diamines to afford a series of cPI films. By virtue of high linearity of main chains and formation of hydrogen bonds derived from amide

Table 3 Thermal and mechanical properties of the as-synthesized cPI films

Polymer	Imidization method[a]	T_g (°C)	$T_{d5\%}$ (°C)	R_w (%)	σ_m (MPa)	ε_b (%)	E_t (GPa)
AMDA/TFDB	C	333	502	53.6	193 ± 17.0	29 ± 9.8	3.9 ± 0.9
	T	356	482	51.6	164 ± 15.7	10 ± 1.7	2.6 ± 0.7
AMDA/*t*-CHDA	T	350	456	25.8	153 ± 11.8	9.0 ± 2.6	3.2 ± 0.3
p-DAMDA/TFDB	T	334	457	50.9	155 ± 10.4	13 ± 5.3	3.0 ± 1.1
IAMDA/TFDB	C	344	492	52.7	170 ± 9.6	46 ± 7.2	3.5 ± 0.5
	T	345	483	49.0	144 ± 22.8	13 ± 1.3	1.8 ± 0.3
IAMDA/*t*-CHDA	T	354	457	21.3	148 ± 14.2	12 ± 3.6	2.0 ± 0.3

[a] C: Chemical imidization; T: thermal imidization.

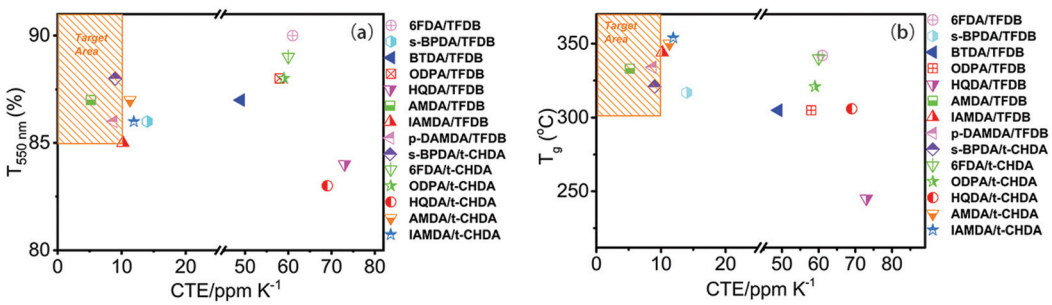

Fig. 10 The relationship between the (a) optical transmittance ($T_{550\ nm}$) and CTE values and between (b) glass transition temperature (T_g) and CTE values of TFDB-based and *t*-CHDA based cPI films.

Published on 26 August 2021. Downloaded on 2/20/2026 2:46:30 PM.

groups, the cPI films exhibited low CTE values (<15 ppm K^{-1}), excellent optical performance ($T_{550\ nm}$ > 85%), great heat resistance (T_g > 300 °C) and sufficient mechanical performance. Of all the as-synthesized cPI films, chemically imidized AMDA/TFDB exhibited the optimal results combining thermal properties with optical performance. To be specific, the AMDA/TFDB(C) film had high optical transmittance of 87% at 550 nm, ultra-low CTE value of 5.2 ppm K^{-1} and high T_g value of 333 °C. In addition, AMDA/TFDB(C) showed high tensile strength of 193 MPa and great flexibility (ε_b = 29%). The results proved that the incorporation of amide groups within polyimide chains led to a significant improvement of thermal and mechanical properties. Therefore, the as-synthesized cPI films are promising for application as cover windows, touch sensor panels or substrates in the field of OLED displays.

Conflicts of interest

There are no conflicts to declare.

Acknowledgements

This work is supported by the National Key R&D Program of China (No. 2017YFB0404700).

References

1 Y. Wang, J. Zhou, X. Chen, J. Sun and Q. Fang, New Colorless and Transparent Poly(ether imide) Derived from a Biobased Plant Oil (Anethole): Synthesis and Properties, *ACS Sustainable Chem. Eng.*, 2019, **7**(13), 11728–11734.

2 C. Yi, W. Li, S. Shi, K. He, P. Ma, M. Chen and C. Yang, High-temperature-resistant and colorless polyimide: Preparations, properties, and applications, *Sol. Energy*, 2020, **195**, 340–354.

3 Q. H. Lu and F. Zheng, *Polyimides for Electronic Applications*. 2018, pp. 195–255.

4 N. Hong, R. A. Synowicki and J. N. Hilfiker, Mueller matrix characterization of flexible plastic substrates, *Appl. Surf. Sci.*, 2017, **421**, 518–528.

5 Z. X. Kang, Y. Zhang and M. Q. Zhou, AgNPs@CNTs/Ag hybrid films on thiolated PET substrate for flexible electronics, *Chem. Eng. J.*, 2019, **368**, 223–234.

6 M. D. Mamo, E.-S. Shin and Y.-Y. Noh, Self-aligned patterning of conductive films on plastic substrates for electrodes of flexible electronics, *J. Mater. Chem. C*, 2017, **5**(41), 10900–10906.

7 S. Cui, Z. Mei, Y. Zhang, H. Liang and X. Du, Room-temperature fabricated amorphous Ga_2O_3 high-response-speed solar-blind photodetector on rigid and flexible substrates, *Adv. Opt. Mater.*, 2017, **5**(19), 1700454.

8 T. Adachi, S. S. Latthe, S. W. Gosavi, N. Roy, N. Suzuki, H. Ikari, K. Kato, K. I. Katsumata, K. Nakata, M. Furudate, T. Inoue, T. Kondo, M. Yuasa, A. Fujishima and C. Terashima, Photocatalytic, superhydrophilic, self-cleaning TiO_2 coating on cheap, light-weight, flexible polycarbonate substrates, *Appl. Surf. Sci.*, 2018, **458**, 917–923.

9 L. Ai, J. Zhang, X. Li, X. Zhang, Y. Lu and W. Song, Universal low-temperature process for preparation of multifunctional high-performance antireflective mesoporous silica coatings on transparent polymeric substrates, *ACS Appl. Mater. Interfaces*, 2018, **10**(5), 4993–4999.

10 M. Hasegawa, T. Hirai, T. Ishigami, S. Takahashi and J. Ishii, Optically transparent aromatic poly(ester imide)s with low coefficients of thermal expansion. 2: Effect of the introduction of alkyl-substituted p-biphenylene units, *Polym. Int.*, 2018, **67**(4), 431–444.

11 D. J. Liaw, K. L. Wang and F. C. Chang, Novel organosoluble poly(pyridine-imide) with pendent pyrene group: Synthesis, thermal, optical, electrochemical, electrochromic, and protonation characterization, *Macromolecules*, 2007, **40**(10), 3568–3574.

12 Y. Liu, J. Guo, J. Wang, X. Zhu, D. Qi, W. Li and K. Shen, A novel family of optically transparent fluorinated hyperbranched polyimides with long linear backbones and bulky substituents, *Eur. Polym. J.*, 2020, **125**, 109526.

13 N. Mushtaq, Q. Wang, G. Chen, B. Bashir, H. Lao, Y. Zhang, L. R. Sidra and X. Fang, Synthesis of polyamide-imides with different monomer sequence and effect on transparency and thermal properties, *Polymer*, 2020, **190**, 122218.

14 M. Hasegawa, S. Takahashi, S. Tsukuda, T. Hirai, J. Ishii, Y. Yamashina and Y. Kawamura, Symmetric and asymmetric spiro-type colorless poly(ester imide)s with low coefficients of thermal expansion, high glass transition temperatures, and excellent solution-processability, *Polymer*, 2019, **169**, 167–184.

15 Z. Chen, S. Zhang, Q. Feng, Y. Wu, S. Liu and J. Zhao, Improvement in mechanical and thermal properties of transparent semi-aromatic polyimide by crosslinking, *Macromol. Chem. Phys.*, 2020, 2000085.

16 G. L. Jiang, D. Y. Wang, H. P. Du, X. Wu, Y. Zhang, Y. Y. Tan, L. Wu, J. G. Liu and A. X. Zhang, Reduced coefficients of linear thermal expansion of colorless and transparent semi-alicyclic polyimide films via incorporation of rigid-rod amide moiety: preparation and properties, *Polymers*, 2020, **12**(2), 413.

17 L. Tao, H. Yang, J. Liu, L. Fan and S. Yang, Synthesis and characterization of highly optical transparent and low dielectric constant fluorinated polyimides, *Polymer*, 2009, **50**(25), 6009–6018.

18 L. Zhai, S. Y. Yang and L. Fan, Preparation and characterization of highly transparent and colorless semi-aromatic polyimide films derived from alicyclic dianhydride and aromatic diamines, *Polymer*, 2012, **53**(16), 3529–3539.

19 H. S. Bi, X. X. Zhi, P. H. Wu, Y. Zhang, L. Wu, Y. Y. Tan, Y. J. Jia, J. G. Liu and X. M. Zhang, Preparation and characterization of semi-alicyclic polyimide resins and the derived alignment layers for liquid crystal display technology, *Polymers*, 2020, **12**(1), 217.

 This journal is © The Royal Society of Chemistry 2021

Published on 26 August 2021. Downloaded on 2/20/2026 2:46:30 PM.

20 X. Wu, C. Shu, X. He, S. Wang, X. Fan, Z. Yu, D. Yan and W. Huang, Optically transparent and thermal-stable polyimide films derived from a semi-aliphatic diamine: synthesis and properties, *Macromol. Chem. Phys.*, 2020, **221**(5), 1900506.

21 J. Miao, X. Hu, X. Wang, X. Meng, Z. Wang and J. Yan, Colorless polyimides derived from adamantane-containing diamines, *Polym. Chem.*, 2020, **11**(37), 6009–6016.

22 Z. H. Wang, G. Q. Fang, J. J. He, H. X. Yang and S. Y. Yang, Semi-aromatic thermosetting polyimide resins containing alicyclic units for achieving low melt viscosity and low dielectric constant, *React. Funct. Polym.*, 2020, **146**, 104411.

23 X. Hu, J. Yan, Y. Wang, H. Mu, Z. Wang, H. Cheng, F. Zhao and Z. Wang, Colorless polyimides derived from 2R,5R,7S,10S-naphthanetetracarboxylic dianhydride, *Polym. Chem.*, 2017, **8**(39), 6165–6172.

24 M. Hasegawa, M. Fujii, J. Ishii, S. Yamaguchi, E. Takezawa, T. Kagayama and A. Ishikawa, Colorless polyimides derived from 1S,2S,4R,5R-cyclohexanetetra carboxylic dianhydride, self-orientation behavior during solution casting, and their optoelectronic applications, *Polymer*, 2014, **55**(18), 4693–4708.

25 M. Hasegawa, Development of solution-processable, optically transparent polyimides with ultra-low linear coefficients of thermal expansion, *Polymers*, 2017, **9**(10), 520.

26 T. Ogura and M. Ueda, Facile synthesis of semiaromatic poly(amic acid)s from trans-1,4-cyclohexanediamine and aromatic tetracarboxylic dianhydrides, *Macromolecules*, 2007, **40**(10), 3527–3529.

27 P. K. Tapaswi, M. C. Choi, Y. S. Jung, H. J. Cho, D. J. Seo and C. S. Ha, Synthesis and characterization of fully aliphatic polyimides from an aliphatic dianhydride with piperazine spacer for enhanced solubility, transparency, and low dielectric constant, *J. Polym. Sci., Part A: Polym. Chem.*, 2014, **52**(16), 2316–2328.

28 Y. Tian, L. Luo, Q. Yang, L. Zhang, M. Wang, D. Wu, X. Wang and X. Liu, Construction of stable hydrogen bonds at high temperature for preparation of polyimide films with ultralow coefficient of thermal expansion and high Tg, *Polymer*, 2020, **188**, 122100.

29 M. Lian, X. Lu and Q. Lu, Synthesis of superheat-resistant polyimides with high T_g and low coefficient of thermal expansion by introduction of strong intermolecular interaction, *Macromolecules*, 2018, **51**(24), 10127–10135.

30 G. Song, C. Chen, X. Wang and J. Yao, Synthesis and properties of polyimides derived from 2,2′-dichloro-4,4′,5,5′-biphenyltetracarboxylic dianhydride, *Polymer*, 2019, **183**, 121862.

31 L. Bai, L. Zhai, M. He, C. Wang, S. Mo and L. Fan, Preparation of heat-resistant poly(amide-imide) films with ultralow coefficients of thermal expansion for optoelectronic application, *React. Funct. Polym.*, 2019, **141**, 155–164.

32 M. Hasegawa, Y. Tsujimura, K. Koseki and T. Miyazaki, Poly(ester imide)s possessing low CTE and low water absorption (II). effect of substituents, *Polym. J.*, 2007, **40**(1), 56–67.

33 M. Hasegawa and N. Koyanaka, Polyimides containing trans-1,4-cyclohexane unit. Polymerizability of their precursors and Low-CTE, low-K and high-T_g properties, *High Perform. Polym.*, 2003, **15**(1), 47–64.

34 M. Hasegawa, Y. Watanabe, S. Tsukuda and J. Ishii, Solution-processable colorless polyimides with ultralow coefficients of thermal expansion for optoelectronic applications, *Polym. Int.*, 2016, **65**(9), 1063–1073.

35 T. Matsuura, Y. Hasuda, S. Nishi and N. Yamada, Polyimide derived from 2,2′-bis(trifluoromethyl)-4,4′-diaminobiphenyl .1. synthesis and characterization of polyimides prepared with 2,2-bis(3,4-dicarboxyphenyl)hexafluoropropane dianhydride or pyromellitic dianhydride, *Macromolecules*, 1991, **24**(18), 5001–5005.

36 H. Liu, L. Zhai, L. Bai, M. He, C. Wang, S. Mo and L. Fan, Synthesis and characterization of optically transparent semi-aromatic polyimide films with low fluorine content, *Polymer*, 2019, **163**, 106–114.

37 C. Y. Guo, J. G. Liu, L. M. Yin, M. G. Huangfu, Y. Zhang, X. Wu and X. M. Zhang, Preparation and characterization of electrospun polyimide microfibrous mats with high whiteness and high thermal stability from organo-soluble polyimides containing rigid-rod moieties, *Fibers Polym.*, 2018, **19**(8), 1706–1714.

38 M. C. Choi, J. Wakita, C. S. Ha and S. Ando, Highly transparent and refractive polyimides with controlled molecular structure by chlorine side groups, *Macromolecules*, 2009, **42**(14), 5112–5120.

39 M. Hasegawa, T. Matano, Y. Shindo and T. Sugimura, Spontaneous molecular orientation of polyimides induced by thermal imidization .2. In-plane orientation, *Macromolecules*, 1996, **29**(24), 7897–7909.

40 S. Numata and T. Miwa, Thermal-expansion coefficients and moduli of uniaxially stretched polyimide films with rigid and flexible molecular chains, *Polymer*, 1989, **30**(6), 1170–1174.

41 J. H. Jou and P. T. Huang, Effect of thermal curing on the structures and properties of aromatic polyimide films, *Macromolecules*, 1991, **24**(13), 3796–3803.

42 S. Ando, M. Harada, T. Okada and R. Ishige, Effective reduction of volumetric thermal expansion of aromatic polyimide films by incorporating interchain crosslinking, *Polymers*, 2018, **10**(7), 761.

43 T. Okada, R. Ishige and S. Ando, Effects of chain packing and structural isomerism on the anisotropic linear and volumetric thermal expansion behaviors of polyimide films, *Polymer*, 2018, **146**, 386–395.

44 S. Dal Kim, B. Lee, T. Byun, I. S. Chung, J. Park, I. Shin, N. Y. Ahn, M. Seo, Y. Lee, Y. Kim, W. Y. Kim, H. Kwon, H. Moon, S. Yoo and S. Y. Kim, Poly(amide-imide) materials for transparent and flexible displays, *Sci. Adv.*, 2018, **4**(10), eaau1956.

45 M. Lian, F. Zheng, X. Lu and Q. Lu, Tuning the heat resistance properties of polyimides by intermolecular inter-

action strengthening for flexible substrate application, *Polymer*, 2019, **173**, 205–214.

46 Y. Oishi, S. Onodera, J. Oravec, K. Mori, S. Ando, Y. Terui and K. Maeda, Synthesis of fluorine-containing wholly alicyclic polyimides by in situ silylation method, *J. Photopolym. Sci. Technol.*, 2003, **16**(2), 263–266.

47 Y. Oishi, N. Kikuchi, K. Mori, S. Ando and K. Maeda, Synthesis of alicyclic polyimides from fluorinated alicyclic diamine, *J. Photopolym. Sci. Technol.*, 2002, **15**(2), 213–214.

Published on 26 August 2021. Downloaded on 2/20/2026 2:46:30 PM.

This journal is © The Royal Society of Chemistry 2021